Frequency and temperature dependence of the microwave surface impedance of $YBa_2Cu_3O_{7-\delta}$ thin films in a dc magnetic field: Investigation of vortex dynamics

Nathan Belk
Department of Physics, Massachusetts Institute of Technology, Cambridge, Massachusetts 02139-4307; Lincoln Laboratory, Massachusetts Institute of Technology, Lexington, Massachusetts 02173-9108; and Rome Laboratory, Hanscom Air Force Base, Massachusetts 01731-3010

D. E. Oates
Lincoln Laboratory, Massachusetts Institute of Technology, Lexington Massachusetts 02173-9108, and Department of Physics, Massachusetts Institute of Technology, Cambridge, Massachusetts 02139-4307

D. A. Feld
Lincoln Laboratory, Massachusetts Institute of Technology, Lexington, Massachusetts 02173-9108

G. Dresselhaus
Francis Bitter National Magnet Laboratory, Massachusetts Institute of Technology, Cambridge, Massachusetts 02139-4307 and Rome Laboratory, Hanscom Air Force Base, Massachusetts 01731-3010

M. S. Dresselhaus
Department of Electrical Engineering and Computer Science and Department of Physics, Massachusetts Institute of Technology, Cambridge, Massachusetts 02139-4307

(Received 31 July 1995; revised manuscript received 18 September 1995)

We report the results of a study of the complex microwave surface impedance Z_S resulting from vortex motion in $YBa_2Cu_3O_{7-\delta}$ thin films in a dc magnetic field applied parallel to the film c axis. Using the technique of stripline resonators we have measured Z_S at frequencies from 1.2 to 22 GHz and at temperatures from 5 to 65 K in magnetic fields from 0 to 4 T. We find that both the surface resistance R_S and the surface reactance X_S increase almost linearly with the magnetic field. In zero applied magnetic field we find the frequency dependence of the surface resistance to be f^2. In the mixed state, however, there is a significant increase in R_S, particularly at lower frequencies, causing R_S to be approximately proportional to $f^{1.2}$ at all measured temperatures. We show that fits of these data to models which include only a single pinning energy and a single characteristic pinning frequency are not able to explain our results. We propose that these data indicate the existence of a large number of metastable bound vortex states separated by energy barriers U_b whose magnitudes extend from $U_b \sim 0$ K to several hundred K, and that the dominant part of R_S arises from vortex transitions between these states.

I. INTRODUCTION

Not long after the discovery of high-temperature superconductivity, it became clear that understanding the behavior of high-T_c materials in magnetic fields would present a considerable challenge. Since the extent of the practical application of high-T_c superconductors will in part be determined by these behaviors, there is great potential benefit to be gained through study of the relationship between the underlying physics in these materials and their in-field properties. The behavior of high-T_c materials in magnetic fields has been probed experimentally through a number of techniques such as torsional oscillators,[1] low-frequency ac magnetic permeability,[2,3] and microwave measurements of the complex surface impedance at both low and high microwave power levels.[4–6] To date, these measurements have shown a rich variety of phenomena which vary greatly, depending on the time scale of the measurement and the temperature range in which the measurements are made.

Our use of stripline resonators[7–9] allows us to measure both the real part R_S and the imaginary part X_S of the microwave surface impedance Z_S of high quality epitaxial thin films at frequencies from 1.2 to 22 GHz. This impedance depends critically on both the amplitude and phase of the vortex motion with respect to the applied rf field $H_{\rm rf}$.

We present the results of a comprehensive investigation of the microwave Z_S of $YBa_2Cu_3O_{7-\delta}$ (YBCO) in the mixed state in magnetic fields from 0 to 4 T applied parallel to the c axis, for temperatures from 5 to 65 K, which are well below $T_c \approx 90$ K for the YBCO films measured in this work. Our results show that the application of the magnetic field causes R_S to increase significantly, particularly at low frequencies. Figure 1 shows R_S as a function of reduced temperature T/T_c at a dc magnetic field of 2 T for the first (sample No. 1) of the two samples we will discuss below. In all of our results the part of R_S which results from the presence of the external field has a relatively strong temperature dependence even at low temperatures and is found to increase with frequency with an approximately $f^{1.2}$ dependence at all fields and temperatures. Further, we find that Z_S is linearly proportional to the magnetic field, indicating that we

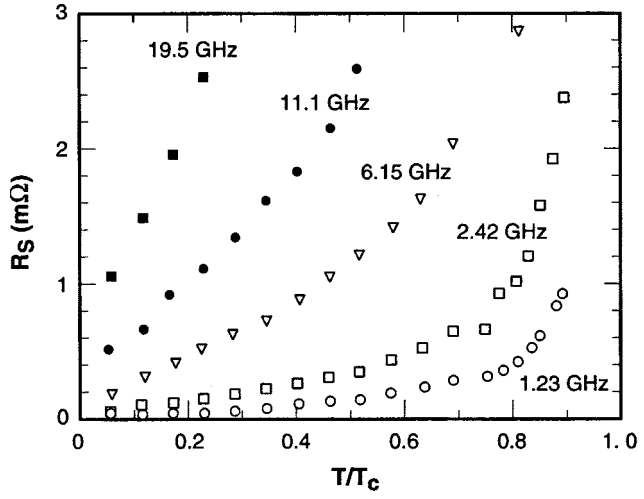

FIG. 1. R_S vs reduced temperature T/T_c in a 2-T magnetic field for sample No. 1 at five different frequencies: (○) 1.23 GHz, (□) 2.42 GHz, (△) 6.15 GHz, (●) 11.1 GHz, (■) 19.5 GHz.

are not probing collective effects, but rather the interactions of individual vortices with point defects in YBCO and that the length scales of these interactions are probably on the order of the coherence length ξ.[3,10–12]

We discuss our data in terms of two models of vortex dynamics. The first model assumes that the pinning potential is uniform and that there are two contributions to vortex energy dissipation: a component due to pinned vortices and a contribution from a small number of vortices which have been thermally depinned in the temperature range studied.[13–15] The second model assumes that the potential is random and that, while the majority of the vortices are strongly pinned, some of the vortices are pinned in metastable states separated by energy barriers.[16] In both models the strongly pinned vortices are expected to dissipate energy with an f^2 dependence at frequencies below the vortex pinning frequency[17] f_P, the frequency at which viscosity no longer allows the vortices to move fast enough to remain in phase with $H_{\rm rf}$. In the uniform potential model, the thermally depinned vortices are expected to be important only at lower frequencies in this temperature range because their contribution to R_S is independent of frequency; at temperatures between 5 and 65 K, almost all of the vortices are pinned.[15] In the model which takes the potential to be random, the low-frequency vortex energy dissipation results from vortex transitions between metastable states and leads to $R_S \sim f$.

We show that although both models provide a reasonable description of our X_S data, a random potential model explains our R_S data much more readily than a uniform potential model. Our results suggest that in the frequency and temperature regime of these experiments, the $R_S \sim f^{1.2}$ data cannot be understood in terms of a sum of $R_S \propto f^2$ and $R_S \propto f^0$ components described by uniform potential models. Models which are based on a simple sum of these loss mechanisms do not fully describe the vortex interactions with pinning sites in the samples and do not accurately treat all the important mechanisms by which energy from the $H_{\rm rf}$ field is dissipated by vortices. We propose that at frequencies between 1 and 20 GHz we are probing small vortex displacements which are on the order of the coherence length ξ and which result in small random variations in vortex energies.[18] In order to explain our results, it is necessary to consider disorder on these short length scales.

This disorder arises in part from the pinning of segments of vortex cores by a random distribution of point defects of volume $D_v \ll \xi^3$ in the YBCO samples.[3,10–12] Because these pinning centers are small, the range of the pinning interactions r_f is roughly the vortex core size ξ so that vortex displacements of $\sim \xi$ can move a segment of a vortex core to a new pinning energy minimum. Further, since the characteristic dimensions of such defects are $< \xi$, individually they cause only small variations in the sample order parameter. As a result, they only slightly reduce the variations in the order parameter due to the presence of the vortex core and therefore the energy gained in pinning the core by a point defect is only a few K. We propose that the random distribution of these defects results in a large number of closely spaced energy minima separated by a random distribution of energy barriers with magnitudes extending down to ≈ 0 K. This results in a broad distribution of characteristic frequencies for the activation of vortex segments between metastable states. It is this distribution of characteristic frequencies that can explain the frequency, temperature, and field dependences of R_S and X_S that are exhibited in our data.

II. EXPERIMENTAL METHODS

The microwave surface impedance data were obtained in a liquid He cryostat fitted with a 9-T superconducting magnet operating in a persistent current mode to ensure field stability. The samples were zero-field cooled to eliminate the possibility of trapped flux. The data presented were obtained at fields much greater than the lower critical field B_{c1} to assure uniform penetration of our microwave resonators by the external field, as verified through the use of a Hall effect sensor.[19]

The samples were mounted in gold-plated copper packages which were fixed to a carbon glass thermometer and mounted in a copper enclosure, which had a heater attached to its base. The temperature was monitored and controlled to obtain temperature stabilities of a few parts in 10^4.

The surface resistance and reactance data reported in this paper were obtained from two YBCO samples grown on $LaAlO_3$ substrates. The two samples were grown by different techniques. Sample No. 1 was 2500 Å thick and was produced through off-axis magnetron sputtering.[20,21] Sample No. 2 was 5800 Å thick and was produced through cylindrical magnetron sputtering.[22] The properties of these films are listed in Table I. Both samples are high quality epitaxial single-phase films with the c axis perpendicular to the plane. All films were patterned with the use of standard photolithographic processes, and were then etched in a 0.25% phosphoric acid solution.

The microwave properties were studied through the use of stripline resonators,[7,8] which are especially useful for studies of the frequency dependence of the surface impedance. These devices support standing waves whose microwave current has the form $I_{\rm rf} = I_0 \sin(n\pi z/s)$ where n is the mode number and z is the position along the length s of the reso-

TABLE I. Parameters of the films determined from both dc (four-point measurements) and microwave measurements. The penetration depth at $T=0$ K and in zero applied dc magnetic field $\lambda(0)$ is the parameter of a two-fluid model fit to our experimental points.

	dc properties		rf properties						
Sample No.	d (μm)	T_c ($R=0$)	T_1 (K)	T_2 (K)	$\alpha_P(0)$[a] (N/m^2)	f_1 (GHz)	T (K)	R_S (Ω)	$\lambda(0)$ (Å)
1	0.24	91	78.5	40.7	3.6×10^5	1.23	5	2.5×10^{-5}	2650
						1.23	20	6.5×10^{-5}	
						1.23	65	2.9×10^{-4}	
2	0.58	89	75.8	23	9.7×10^5	1.47	5	1.2×10^{-5}	2340
						1.47	20	2.8×10^{-5}	
						1.47	65	1.4×10^{-4}	

[a]Extrapolated to $T=0$ K, assuming that $U_P \gg kT$.

nator. The resonant frequency for the modes is $f_n=nf_1$, where f_1, is the lowest-frequency mode, which ranges from 1.2 to 1.5 GHz. The measurements were performed using a vector network analyzer, and the highest-frequency modes which could be measured were about 22 GHz. To prevent radiation losses, the resonators were sandwiched between two superconducting ground planes which formed the top and bottom of a microwave cavity. The sides of the cavity were formed by a gold-plated copper package in which the resonator and ground planes were mounted. The resonator, ground planes, and orientation of the applied field are shown in Fig. 2. At most measurement frequencies, the dynamics of the stripline completely dominates those of the surrounding cavity. However, some of the modes of the resonator are at frequencies very close to the modes of the cavity, and the resulting coupling makes them unsuitable for these experiments. Any residual cavity interactions with the remaining modes were eliminated by subtracting the small zero field R_S from the in field R_S at each frequency.

The striplines were weakly coupled so that microwave signals could be applied to the resonator at one end and monitored at the other, while not significantly reducing the Q of the device. Stripline widths were selected so that at the frequency f_1 each resonator had a zero-field low-temperature Q of about 10^5. This allowed measurement of the frequency dependence of both the reactive X_S and the resistive R_S part of the Z_S of these films to an accuracy of as much as 1 part in 10^5.

The microwave losses in the $LaAlO_3$ substrates, defined in terms of a loss tangent, produce a change in the resonator Q given by $1/Q_m=1/Q+\tan\delta$, where Q_m is the measured Q and $\tan\delta\approx5\times10^{-6}$. This correction is small enough so that it is not significant in this work.[7,19,23] The shifts in resonant frequencies due to the changes in the Q of the resonator are of order $1/Q^2$ and are always negligible in comparison to the shifts we measure due to the changes in sample's reactance. Further, all of our data were taken with the microwave current kept low enough so that the surface resistance is independent on the rf power level.

As we shall discuss below, Z_S in these samples is determined by the complex microwave penetration depth $\tilde{\lambda}$ in these films. The real part of the zero-field microwave penetration depth $\tilde{\lambda}_R(0)$ is essentially equal to the London penetration depth λ_L at these frequencies. The imaginary part $\tilde{\lambda}_I(0)$ is proportional to R_S. We extract $\tilde{\lambda}_R$ from our measurements of the mode frequencies which are determined by the stripline inductance L, which has a geometrical component L_g and a kinetic component L_k which depends on $\tilde{\lambda}_R$ and on film thickness d. To obtain $L(\tilde{\lambda}_R)$ we have used the

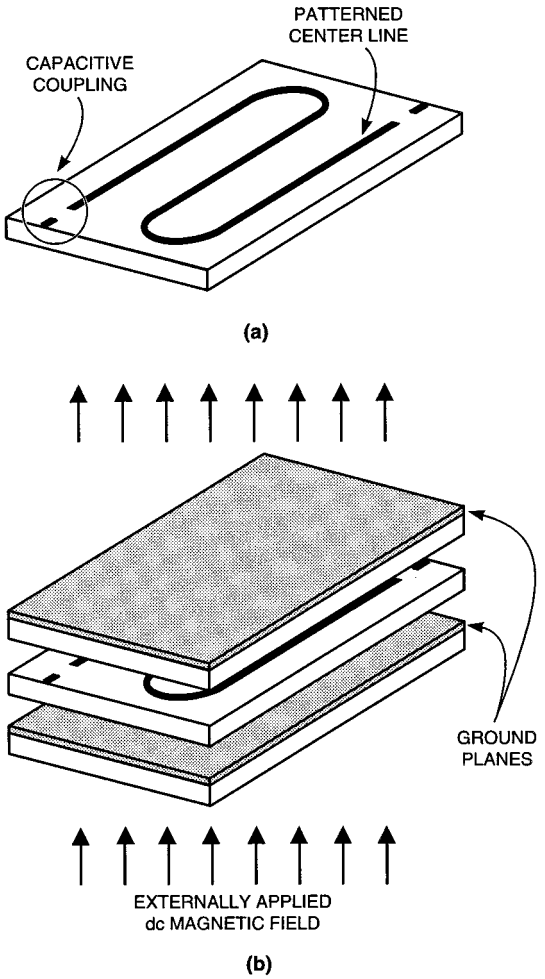

FIG. 2. View of the structure of a stripline resonator. (a) Patterned resonator line. The rf current flows in the x-z plane parallel to the resonator line. (b) View of the resonator plus ground planes which form the top and bottom of the resonator cavity. The dc magnetic field is in the y direction parallel to the c axis.

results of Sheen *et al.*[8] The shifts in the resonant frequencies are then

$$\Delta f_n = \frac{-f_{n0}}{2L}\left(\frac{L_{n0}}{L}\right)^{1/2}\left[\frac{d}{d\tilde{\lambda}_R}L(\tilde{\lambda}_R)\right]\Delta\tilde{\lambda}_R, \tag{1}$$

where f_{n0} and L_{n0} are, respectively, the zero-temperature zero-field frequency and inductance of a resonant mode n. Because $\Delta\tilde{\lambda}_R$ is proportional to Δf_n and ΔX_S, we will generally quote the ΔX_S in the presentation of the data.

We obtain $\tilde{\lambda}_R(0)$ and the zero-field transition temperature T_c by incorporating the expression for the penetration depth taken from the two-fluid model[7,23,24]

$$\tilde{\lambda}_R(T) = \frac{\tilde{\lambda}_R(0)}{\left[1-\left(\frac{T}{T_c}\right)^4\right]^{1/2}} \tag{2}$$

into $L(\tilde{\lambda}_R)$ in Eq. (1) to obtain the frequency shift Δf_n for a given mode as a function of T. The parameters $\tilde{\lambda}_R(0)$ and T_c are varied to fit the frequency versus temperature data for the first mode.

The surface resistance R_S, which is proportional to the imaginary part of the microwave penetration depth $\tilde{\lambda}_I$, was extracted from the Q of a mode and the frequency f_n using the relationship[8]

$$R_S = \frac{\mathcal{G}(\tilde{\lambda}_R/d)f_n}{Q}, \tag{3}$$

where the geometric function $\mathcal{G}(\tilde{\lambda}_R/d)$ accounts for the finite ratio of the film thickness d to $\tilde{\lambda}_R$.[7,8] The function $\mathcal{G}(\tilde{\lambda}_R/d)$ also takes into account the stripline geometry, the characteristic impedance of the stripline, and the current distribution within the resonator.

III. THEORY

As a result of the use of the correction factors $\mathcal{G}(\tilde{\lambda}_R/d)$ and $L(\tilde{\lambda}_R)$ in Eqs. (1) and (3),[7,8] the R_S and $\tilde{\lambda}_R$ determined from our data yield Z_S for ac currents flowing in a semi-infinite half-plane:

$$Z_S = R_S + iX_S = i\mu_0\omega\tilde{\lambda}. \tag{4}$$

In what follows we present the theories for $\tilde{\lambda}$ for the motion of vortices resulting from a dc magnetic field normal to the plane of the film.

A. $\tilde{\lambda}$ in the absence of vortices

In the absence of vortices the field dependence of the London penetration depth[19] λ_L is given approximately as

$$\lambda_L(B,T) \approx \lambda_L(0,T)\left[1+\frac{B}{2B_{c2}}\frac{1+(T/T_c)^2}{1-(T/T_c)^2}\right], \tag{5}$$

where we have used the Ginzburg-Landau approximation for the upper critical field $B_{c2}(T)$. In our incorporation of this effect we use a typical value of 100 T for $B_{c2}(0)$.[25–28] Because $B/B_{c2} \leqslant 0.03$ for the highest dc fields discussed in this work, the field dependence of λ_L changes our determination of $\Delta\tilde{\lambda}_R$ by less than 10% at typical measurement temperatures. Because the correction to λ_L is not large, we are not sensitive to the exact value and temperature dependence of B_{c2}.

In the absence of vortices the imaginary part of the microwave penetration depth resulting from normal fluid losses in a two-fluid model[18] is given as

$$\tilde{\lambda}_I = \mathrm{Im}\left[\frac{\lambda_L}{(1+2i[\lambda_L/\delta_{\mathrm{NF}}]^2)^{1/2}}\right] \approx \lambda_L\left(\frac{\lambda_L}{\delta_{\mathrm{NF}}}\right)^2, \tag{6}$$

where δ_{NF} is the microwave penetration depth of the normal fluid. In this frequency and temperature regime $\delta_{\mathrm{NF}} \approx 3\ \mu$m and is determined almost entirely by extrinsic effects.[9] Because $\lambda_L/\delta_{\mathrm{NF}} \ll 1$, the effect of the normal fluid losses is almost completely contained in the zero field $R_S(0)$. Thus by subtracting the zero-field $R_S(0)$ data from the in-field $R_S(H)$ data at each temperature and focusing on $\Delta R_S = R_S(H) - R_S(0)$ we can isolate the losses associated with magnetic vortices. Since $\delta_{\mathrm{NF}} \propto 1/f^{1/2}$, its contribution to R_S will have an f^2 frequency dependence. Because this dependence is very different than the $R_S \sim f^{1.2}$ dependence we have measured in all samples and at all temperatures, this component is not important in our measured R_S.

B. $\tilde{\lambda}$ in the mixed state

There are a number of theories which describe the behavior of vortex systems in which some fraction of the vortices is pinned and the rest of the vortices are momentarily freed by thermal activation.[13–15] In these theories, the displacements u of a pinned vortex segment, when driven by an ac current $j = j_0 e^{i\omega t}$ perpendicular to B, are determined by a force balance equation of the form[13–15]

$$i\omega\eta u + \alpha_P u = jB\phi_0 + F(T), \tag{7}$$

where η is the linear vortex viscosity, α_P is the vortex restoring force constant, $\hat{B}$ is the field direction, ϕ_0 is the flux quantum, and $F(T)$ represents thermal fluctuations. It is customary to define the pinning frequency f_P as $\alpha_P/2\pi\eta$. In the Bardeen-Stephen model,[29,30] η is given by the following expression:

$$\eta = \phi_0 B_{c2}/\rho_n \approx 2\times10^{-7}\frac{1-(T/T_c)^2}{1+(T/T_c)^2}\ \mathrm{Ns/m^2}, \tag{8}$$

where the in-plane low-temperature normal-state resistivity ρ_n for YBCO is assumed to be roughly 100 $\mu\Omega$ cm as other authors have suggested.[31,32] There are differing models for the temperature dependence of ρ_n in Eq. (8)[13,27,33] and therefore, the magnitude and temperature dependence of η is somewhat uncertain. Experimentally determined values for $\eta(T=0)$ range from[34,35] $\approx 5\times10^{-8}$ N s/m^2 to[28] $\approx 1\times10^{-6}$ N s/m^2.

The vortex restoring force constant α_P is related to the vortex pinning potential $U(u)$ by the relation

$$\alpha_P \approx \frac{1}{l}\frac{\partial^2 U(u)}{\partial u^2}, \tag{9}$$

where l is the length of the pinned vortex segment. Since, as we will discuss below, our measurements indicate that α_P is

independent of magnetic field,[19] we conclude that α_P is dominated by interactions between individual vortex cores and pinning centers in the YBCO samples. In the simplest approximation, α_P is determined by the condensation energy of the super electrons displaced by the pinning center and is proportional to B_c^2 where B_c is the thermodynamic critical field. In this model the vortex restoring force constant is given by[10,30]

$$\alpha_P(T)=\alpha_P(0)[1-(T/T_c)^2]^2. \tag{10}$$

A more detailed consideration of the scattering of quasiparticles by pinning centers which result from point defects[3,12,36] gives a different form for α_P:

$$\alpha_P=\alpha_P(0)\frac{[1-(T/T_c)^2]^2}{(1+T/T_c)^4}. \tag{11}$$

Equation (11) has a strong linear component to the temperature dependence in the limit of low temperatures, and is valid in the absence of background quasiparticle scattering from other nearby sample defects.

1. Coffey-Clem model

The Coffey-Clem model[13] for vortex dynamics adds an additional temperature dependence to α_P which accounts for the effects of thermal fluctuations of the vortices in a uniform periodic potential. In this model α_P is divided by the factor

$$\beta(\nu)=\frac{I_0(\nu)I_1(\nu)}{I_0^2(\nu)-1}, \tag{12}$$

where I_0 and I_1 are modified Bessel functions and $\nu=U_P/2kT$. For temperatures not too close to T_c, $\beta(\nu)$ is ≈ 1. Other similar theories for $\tilde{\lambda}$ do not consider this effect.[14,16]

In addition to the pinned vortices, there are some vortices which become thermally depinned. If the usual assumption is made that the vortices are all pinned in wells of roughly the same depth,[13–15] those vortices will have a contribution ϵ to Z_S which is generally taken to be $\propto\exp\{-U_P/kT\}$.[14,15] In the Coffey-Clem model it is

$$\epsilon=\frac{1}{I_0^2(\nu)}\sim\pi\frac{U_P}{kT}\exp\left(\frac{-U_P}{kT}\right), \tag{13}$$

where U_P is the mean depth of the vortex pinning potential. For $U_P\gg kT$ there is not a significant difference between the various forms for ϵ. The effect of the thermal depinning or the quantum tunneling of vortices can be incorporated into Eq. (7) by multiplying α_P by the factor

$$\kappa=\frac{if/\epsilon f_P}{1+if/\epsilon f_P}. \tag{14}$$

This factor accounts for the reduction of the elastic pinning force density of the vortex lattice.[14]

The motion of the vortices in response to the microwave current j can be described by an ac generalized susceptibility $\chi_{\rm ac}$ which gives the vortex displacement $u=\chi_{\rm ac}j\phi_0$. Equations (7), (12), (13), and (14) can be used to give the complex $\chi_{\rm ac}^{\rm UP}$ for a vortex in a uniform potential:

$$\chi_{\rm ac}^{\rm UP}=\frac{1}{\alpha_P}\frac{\beta(\nu)}{1+i(f/f_P)\beta(\nu)}-\frac{i\epsilon}{f}\frac{2\pi/\eta}{1+i(f/f_P)\beta(\nu)}. \tag{15}$$

Equation (15) is in a form for overdamped harmonic systems with the dominant characteristic frequencies of f_P in the first term and 0 Hz in the second.

2. Koshelev-Vinokur model

The Koshelev-Vinokur model[16] considers the transitions of vortex segments of length l between pairs of metastable states separated by a distance $d_h\sim\xi$ in a random potential. The states are separated by energy barriers and the characteristic frequency for the activation over the barriers is $f_{\rm th}=f_a\exp(-U_b/kT)$ where f_a is an attempt frequency,[37,38] which we take to be $\sim f_P$,[10,26] and U_b is the barrier height. For this random potential model, $\chi_{\rm ac}^{\rm RP}$ is given as

$$\chi_{\rm ac}^{\rm RP}(f,T)=\frac{d_h^2l^2}{4kT}\int_0^\infty\frac{g(U_b)dU_b}{1+i(f/f_a)\exp(U_b/kT)}+\frac{1/\alpha_P}{1+i(f/f_P)}, \tag{16}$$

where $g(U_b)$ is the distribution of energy barriers. We treat the viscous losses due to the majority of vortices which are not hopping between potential minima by including a term to Eq. (16) such as the first term in Eq. (15) with $U_P\gg kT$.

There are several contributions to the temperature dependence of $\chi_{\rm ac}$ obtained from Eq. (16). At a given frequency f, the metastable states for which $f\approx f_{\rm th}$ are those principally responsible for ΔR_S. Since the metastable states have $U_b\sim kT$, any changes in $g(U_b)$ at $U_b\sim kT$ will produce similar changes in ΔR_S. As the typical values of U_b increase with temperature, the differences in the energies between allowed metastable vortex states increase. As a result, the number of available states $g(U_b)$ grows linearly with T. For this reason R_S is expected to grow linearly with T at low temperatures.[16] Another component of the temperature dependence of $\chi_{\rm ac}$ arises from expected increases in both l and d_h with increasing temperature.[16,39]

3. Frequency dependence of Z_S

The velocity v of the driven vortices is given by $v=i\omega\chi_{\rm ac}j\phi_0$. Using this relation for v and the equation for the electric field generated by vortices, $E=\Sigma_i(\phi_0 v_i)=(i\omega B\chi_{\rm ac}\phi_0)j$, we obtain an effective penetration depth in the mixed state for temperatures not too close to T_c:

$$\tilde{\lambda}\approx\left[\lambda_L^2+\frac{B\phi_0}{\mu_0}\chi_{\rm ac}\right]^{1/2}. \tag{17}$$

In Eq. (17) we have neglected the effects of the normal fluid losses [Eq. (6)] which is included directly by subtracting the zero field R_S from the in field R_S as mentioned previously.

In both the uniform and the random potential models, when $B\phi_0\chi_{\rm ac}/\mu_0\ll\lambda_L$ [Eq. (17)], the surface impedance becomes $Z_S\propto if\chi_{\rm ac}$; therefore, for the uniform potential model the second term in Eq. (15) will generate an $R_S\propto f^0$ dependence for the vortices which become thermally depinned. For $U_P\gg kT$, this $R_S\propto f^0$ term is strongly temperature dependent. The first term in Eq. (15) will contribute an $R_S\propto f^2$ dependence for $f<f_P$, while for $f>f_P$ all of the vortices will have an $R_S\propto f^0$. Additionally, at $f=f_P$ there will be a significant

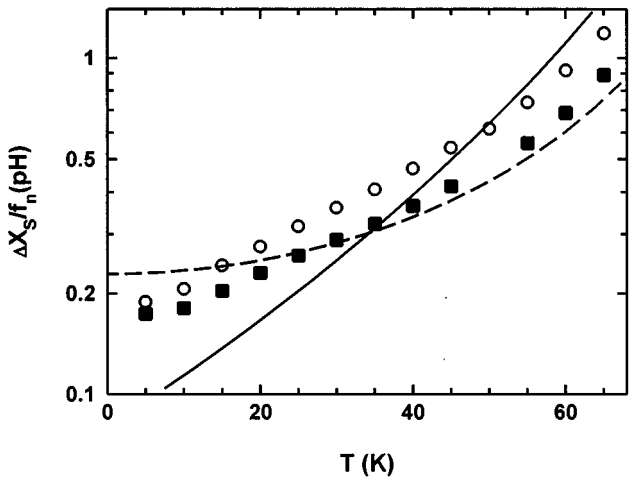

FIG. 3. $\Delta X_S/f_n$ resulting from a 2-T magnetic field at $n=1$ (○) and $n=6$ (■) plotted on a logarithmic scale as a function of temperature for sample No. 1. The solid line is a fit to $\ln(\Delta X_s/f_n)$ for $n=6$ using Eq. (11). The dashed line is the fit using Eq. (10).

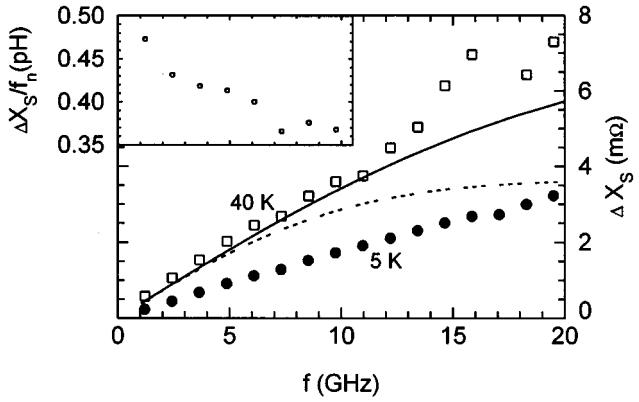

FIG. 4. The ΔX_S in sample No. 1 due to the application of a 2-T magnetic field vs the mode frequency at two temperatures: (●) 5 K, (□) 40 K. The dashed curve shows the ΔX_S calculated using the Coffey-Clem model for $f_P=20$ GHz and the solid curve for $f_P=40$ GHz. The inset to this graph shows the $T=40$ K data replotted as $\Delta X_S/f_n$ vs f_n.

reduction of the vortex contribution to the kinetic inductance, since at f_P the vortices will no longer move rapidly enough to remain in phase with $H_{\rm rf}$. In the random potential model [Eq. (16)] for $f \geqslant f_P$, the vortices behave as they do in the uniform potential model. However, because the temperature dependence for $f_{\rm th}$ and the magnitude of the contribution to $\chi_{\rm ac}$ arising from each $f_{\rm th}$ in the random potential model will be similar, the frequency dependence of Z_S is only weakly temperature dependent. When f is in the range of the thermal frequencies $f_{\rm th}=f_a\exp[-U_b/kT]$, R_S is proportional to f while the vortex contribution to the kinetic inductance L_k is still dominated by the strongly pinned vortices and the effects of the hopping of vortices will be to decrease L_k with increasing frequency at all frequencies. As a result X_S will increase more slowly than f at all frequencies.

IV. EXPERIMENTAL RESULTS

A. Frequency shifts

Figure 3 shows the X_S changes of two resonator modes ($n=1$, 6) divided by the mode frequency $\Delta X_S/f_n$ versus temperature for sample No. 1 resulting from the application of a 2-T magnetic field. These shifts are caused by the increase of $\tilde{\lambda}_R$ which is due to two effects. The first is the small increase to λ_L given by Eq. (5), and the second, the one of interest here, is due to the part of the vortex motion which is in phase with the ac current. At frequencies much less than f_P, the part of $\Delta X_S/f_n$ due to vortices in the measured temperature regime (5–65 K) is given by

$$\Delta X_S/f_n \propto B\ \mathrm{Re}(\chi_{\rm ac}). \tag{18}$$

Because, as we shall discuss below, the vast majority of the vortices is pinned, the real part of $\chi_{\rm ac}$ is proportional to $1/\alpha_P$ [Eq. (15)] in the uniform potential models. In the random potential models, $\mathrm{Re}\chi_{\rm ac}$ also contains an additional contribution due to the activation of vortices between metastable states. The differences between the $\Delta X_S/f_n$ data at the two frequencies reflect the extent to which the vortices in the sample are able to move rapidly enough to remain in phase with $H_{\rm rf}$. As we shall discuss, our results indicate that the larger $\Delta X_S/f_n$ values measured at low frequency arise from a small number of vortex segments which are able to hop between metastable vortex states rapidly enough to follow $H_{\rm rf}$ at $f<7.3$ GHz. For this reason we use $f_n \approx 7.3$ GHz data to determine more accurately the behavior of the pinned vortices. The best-fit functions for $\Delta X_S/f_6 \propto 1/\alpha_P(T)$ from Eqs. (10) and (11) are shown by the dashed and solid lines in Fig. 3. The measured temperature dependence of α_P is different from that predicted by either Eq. (10) or (11). In order to fit the data, α_P must include a low-temperature linear component which is not present in Eq. (10). However, this linear component is not as strong as that predicted by Eq. (11) which considers quasiparticle scattering. The variation of the higher-temperature part of $\alpha_P(T)$ is not as strong as that expected from either Eq. (10) or Eq. (11). Because neither of these equations provides a particularly good fit, we use the empirically determined form

$$\alpha_P(T)=\alpha_P(0)\,\frac{1-(T/T_1)^2}{1+T/T_2} \tag{19}$$

for $\alpha_P(T)$ in the fits to the Coffey-Clem model that follow. The values for T_1 and T_2 obtained empirically for the two samples are given in Table I. Since $\alpha_P(T)$ and $U(T)$ are related by Eq. (9), we expect that the pinning energies U_P will decrease with increasing temperature.

The frequency shifts of the resonator modes ΔX_S for sample No. 1 as a function of frequency at $T=5$ and 40 K (Fig. 4) show the nearly linear f dependence which is exhibited in both samples at these temperatures. Also shown on this graph are the nonlinear frequency shifts ΔX_S predicted by Eq. (17) with α_P determined from the low-frequency slope in Fig. 4 and f_P taken to be 20 GHz (dashed curve) and 40 GHz (solid curve). The high-frequency data for both samples show a more linear frequency dependence than ei-

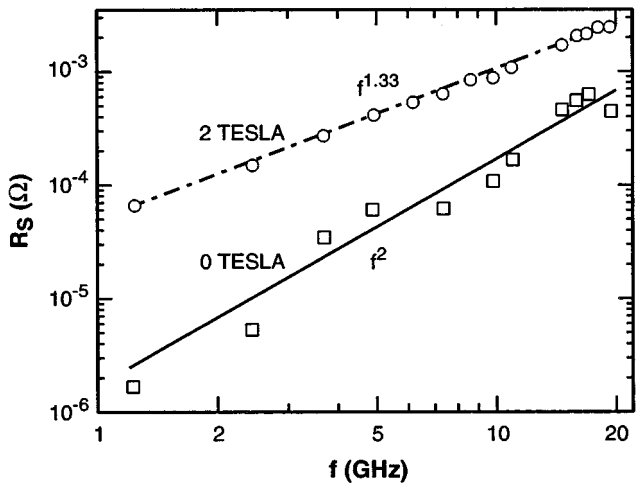

FIG. 5. The surface resistance $R_S(0)$ at 0 T in sample No. 1 (□) and $R_S(H)$ at 2 T (○) vs frequency plotted on a log-log scale. The solid line shows $R_S \propto f^2$, and the dashed line shows $R_S \propto f^{1.33}$.

ther of these curves from roughly 1.4 to 20 GHz. Because $\Delta X_S \propto f\ \mathrm{Re}(\chi_{\mathrm{ac}})$, we conclude from this linear dependence that most of the vortices are moving in phase with H_{rf} at all measured frequencies, so that $f_P = \alpha_P/2\pi\eta$ is greater than 40 GHz for the majority of the vortices in both samples at $T=5$ and 40 K. Because our data show that $f_P \gg f_n$, we are unable to obtain the exact value of f_P from these data. An important feature in the frequency shift data in Fig. 4 is that a linear extrapolation of the 40 K frequency shift data to $f=0$ yields a nonzero Δf intercept. This feature can be seen as the deviation from a horizontal line in the inset of Fig. 4 in which we plot $\Delta X_S/f_n$ vs f_n for the first few modes of the 40 K data in the main figure. As we shall discuss below, the sublinear behavior of ΔX_S causes α_P to be frequency dependent at all frequencies, and results from a small number of vortices being activated between metastable states with characteristic activation frequencies in the range of the measurement frequencies and below.

The frequency shift data from the two samples allow the determination of $\alpha_P(T)$ and show that f_P is greater than 40 GHz for both samples at temperatures less than 40 K. These results put an upper limit on the vortex viscosity and the amount of energy that the pinned vortices can dissipate when a uniform pinning potential is assumed such as in Eq. (17), as we discuss below.

B. Surface resistance

Figure 5 shows R_S for sample No. 1 as a function of frequency at 20 K for $B=0$ T and $B=2$ T. At zero magnetic field the surface resistance follows roughly an f^2 dependence indicated by the solid line, due to the power dissipation by the normal electrons.[7,23,40,41] At 2 T the magnitude of the surface resistance increases substantially, particularly at low frequencies, changing the frequency dependence to roughly $f^{1.33}$ (dashed line). If the zero-field resistance is subtracted from the in-field resistance, then ΔR_S resulting from the vortices is $\propto f^{1.24}$ at 2 T. With the values and functional forms for α_P obtained from the frequency shift data, we have attempted to fit $R_S(f)$ to the Coffey-Clem model, which includes thermal depinning, and provides a frequency dependence of R_S different from the f^2 dependence that describes the surface resistance for pinned vortices alone.

In the fits to the Coffey-Clem model, we use the $\alpha_P(T)$ taken from the $f_n \simeq 7.3$ GHz data since this value accurately reflects the slope of the $\Delta X_S/f_n$ vs f_n data ($\sim 1/\alpha_P$) in Fig. 4. We adjust $\alpha_P(T)$ so that the temperature dependence of the real part of the microwave penetration depth $\tilde{\lambda}_R$, determined from the frequency shift measurements, is consistent with that predicted by the model in the limit that the depth of the vortex pinning potential $U_P \approx 7kT$. This limit is consistent with results of the fits at all measured temperatures as we will discuss. The values of the restoring force constant α_P at 5 K found from the frequency shift measurements at 7.3 GHz for samples Nos. 1 and 2 are roughly 3.6×10^5 N/m^2 and 9.7×10^5 N/m^2, respectively, which are similar to the values found by other authors.[4,30] Because of the factor $\beta(\nu)$ in the Coffey-Clem model [Eqs. (12) and (15)], the values of $\alpha_P(0)$ required to fit the ΔR_S to that model are about 16% larger than those listed in Table I. (Note that the parameters listed in Table I have errors of about 20%.) To eliminate the small components of R_S due to the zero-field losses in the films and possible interactions with the microwave cavity, at each temperature, we subtract the zero field R_S from the in field R_S. To prevent overweighting of the high-frequency data by the fitting algorithm, we fit $\ln(R_S)$ to the $\ln(-i\mu_0\omega\tilde{\lambda}_I)$ data. In the fits, the low-frequency R_S data determine U_P almost entirely, while the high-frequency R_S data determine f_P.

In the fits to the Koshelev-Vinokur model, it is difficult to estimate the temperature dependence for the individual parameters discussed in Sec. III B 2. As discussed previously, the pinning energy of a vortex core tends to have the same temperature dependence as the α_P of a pinned vortex. However, contributions to our measured α_P arise from the hopping of vortices between metastable states. As a result, the actual temperature dependences of α_P and the vortex pinning potential are not known precisely. For simplicity, when fitting our data to Eq. (16), we assumed that $l=100$ Å, $d_h=50$ Å, $f_P=f_a$, and that these four parameters are temperature independent for $T<60$ K. Varying f_P with T would allow the high-frequency ΔR_S to be adjusted independently; however, the fits obtained from the Koshelev-Vinokur model without varying f_P were already quite reasonable. We assume that the distribution of pinning energies at low U_b is given by $g(U_b)=(1+U_b/U_0)/U_0$. The temperature dependence of U_0 we set equal to that of α_P, and the temperature dependence of both parameters is chosen so that the frequency shifts predicted by Eq. (16) are within 10% of the measured frequency shifts.[42] As previously mentioned, when fitting these data we assumed that deviations from $\Delta R_S \propto f$ are due to the $\Delta R_S \propto f^2$ dependence resulting from the viscous losses of the majority of vortices which are not involved in hopping between wells.

The fit to the Coffey-Clem model of the 40 K $\Delta R_S(f)$ data at 3 T for sample No. 2 is shown as the solid line in Fig. 6. The Coffey-Clem model accounts for the high levels of low-frequency dissipation through thermally activated flux creep which contributes a frequency-independent component to ΔR_S. The parameters generated by the fit in Fig. 6 are

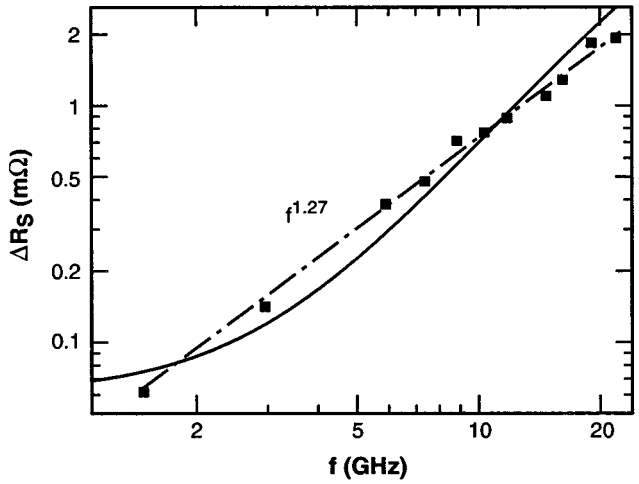

FIG. 6. The surface resistance $\Delta R_S = R_S(H) - R_S(0)$ of sample No. 2 at 3 T and 40 K (■) vs frequency plotted on a log-log scale. The solid curve shows the fit of the Coffey-Clem model to $\ln(\Delta R_S)$. The dashed line shows $\Delta R_S \propto f^{1.27}$.

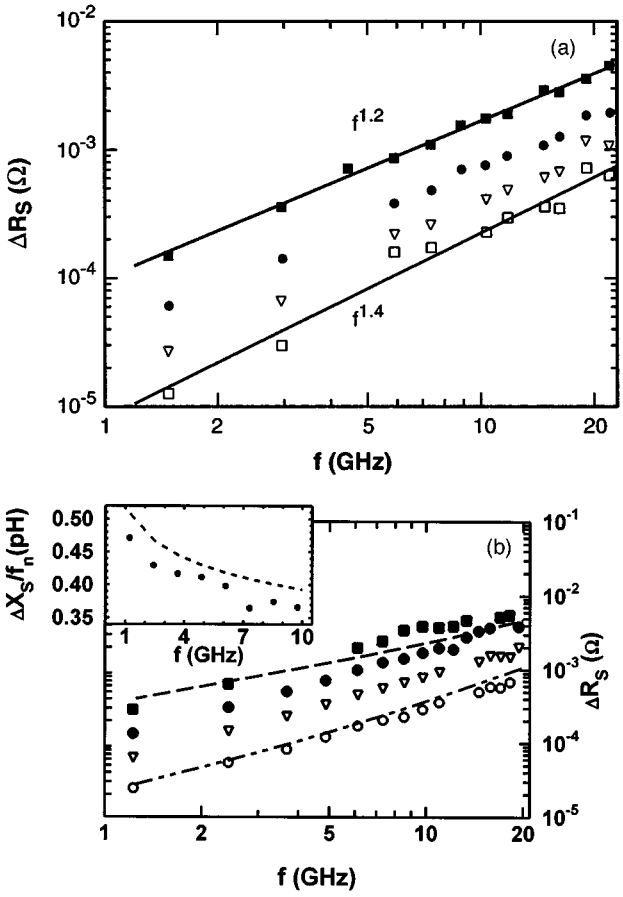

FIG. 7. (a) The surface resistance ΔR_S of sample No. 2 at 3 T as a function of frequency at four different temperatures plotted on a log-log scale: (□) 5 K, (△) 20 K, (●) 40 K, (■) 65 K. The solid lines in (a) are included as reference lines with the indicated slopes. (b) The surface resistance ΔR_S of sample No. 1 at 2 T as a function of frequency at four different temperatures plotted on a log-log scale: (○) 5 K, (△) 20 K, (●) 40 K, (■) 60 K. The dashed lines show the fits of the 5 K and the 60 K data to the random potential model. The inset to this graph shows $\Delta X_S/f_n$ vs f_n predicted for the $T = 40$ K fit of Eq. (16) for the first few f_n.

$U_P/k = 330$ K and $f_P = 45$ GHz. Because $U_P \gg kT$, the low-frequency ΔR_S should have a very strong exponential temperature dependence [Eq. (13)]. Additionally, from $\eta(T)$ and $\alpha_P(T)$ given by Eq. (8) and Eq. (19), respectively, we find that the high-frequency $\Delta R_S \propto \alpha_P^2/\eta$ should have a relatively weak temperature dependence. As a result, the *frequency dependence* of ΔR_S can be expected to be a strong function of temperature in this sample at these temperatures. However, the data indicate the opposite. In the samples tested, the field-induced part of ΔR_S exhibits a predominant form of $\Delta R_S \propto f^{1.2}$ at all fields at temperatures from 5 to 65 K. Figures 7(a) and 7(b) show ΔR_S vs f for several temperatures from 5 to 64 K for sample Nos. 2 and 1, respectively, and it is seen that the slope is essentially independent of temperature. The fit of these data to the Koshelev-Vinokur model is shown for sample No. 1 in Fig. 7(b) for temperatures of 5 and 60 K. The inset to Fig. 7(b) shows the fit to the $\Delta X_S/f_n$ data for the first few modes of sample No. 1. These fits indicate that $U_0(T=0) = 160$ K and both f_P and f_a were taken to be 70 GHz at all temperatures. The normalization of $g(U_b)$ was such that the total fraction of vortices involved in hopping between metastable states at these frequencies and temperatures was about 0.12, though this fraction of vortices may be an overestimate since at 60 K both d_h and l will have grown in Eq. (16).

Using a model which assumes a uniform U_P such as the Coffey-Clem model to fit the sample and temperature-invariant frequency dependence of ΔR_S requires U_P to rise with temperature at $\approx 7kT$, so that the sum of the $\Delta R_S \propto f^0$ for thermally depinned vortices and the $\Delta R_S \propto f^2$ contributions for the pinned vortices always approximate the $\Delta R_S \propto f^{1.2}$ dependence as shown in the simple linear fit to the frequency dependence of the data (see Fig. 6). However, $\alpha_P(T)$ should be proportional to $U_P(T)$ and our frequency shift vs temperature data (Fig. 3) show that α_P decreases as temperature increases. The random potential model naturally generates a $R_S \sim f^1$ dependence as well as a roughly linear temperature dependence at all frequencies.

In models such as that of Coffey and Clem, the high-frequency ΔR_S primarily determines f_P. The temperature dependence of f_P is very different in sample No. 1 from that in sample No. 2. If the empirically determined α_P is used to obtain $\eta \propto \alpha_P/f_P$ from f_P in these samples, then at low temperatures, η must increase linearly with temperature in sample No. 1 and decrease linearly with temperature in sample No. 2. Further, the fits to ΔR_S at $T \geqslant 40$ K generate values of $f_P \leqslant 20$ GHz for sample No. 1 while, as discussed above, the linearity of the ΔX_S vs f data (Fig. 4) shows that $f_P \geqslant 40$ GHz for the majority of vortices in both samples at 40 K.

The drop in f_P with increasing temperature for samples Nos. 1 and 2, which is indicated by the fits to the Coffey-Clem model, reflects the roughly linear temperature dependence of ΔR_S in both samples at $T \leqslant 40$ K at all measured frequencies. In order to show this more clearly, we take the ΔR_S data of sample No. 1 (Fig. 1) from which we subtract the zero-field ΔR_S data and we then plot $\Delta R_S/f_n^{1.2}$ vs T in

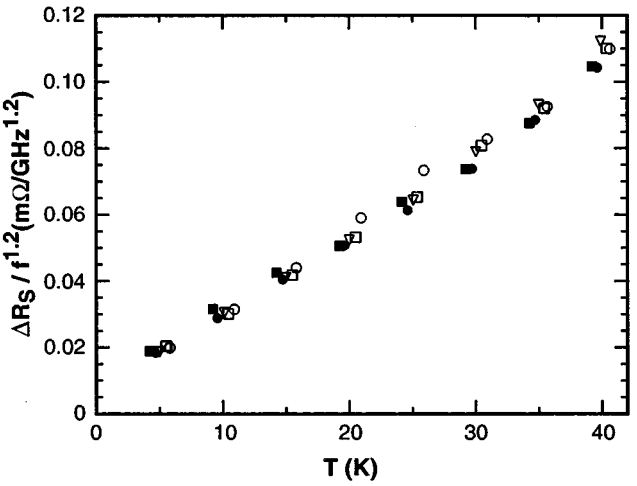

FIG. 8. The ΔR_S of sample No. 1 divided by $f^{1.2}$ at temperatures from 5 K to 40 K in 5-K intervals for five different frequencies: (■) $f=1.23$ GHz, (●) $f=2.43$ GHz, (△) $f=6.15$ GHz, (□) $f=11.1$ GHz, and (○) $f=19.5$ GHz. The points are offset in temperature for clarity in presentation.

Fig. 8. The similarity of the slopes of the $\Delta R_S/f_n^{1.2}$ vs T curves in Fig. 8 indicates that the component of ΔR_S which has the strong linear temperature dependence grows like $f^{1.2}$. If the data were plotted as $\Delta R_S/f^{1.4}$, the slope of the $f=1.23$ GHz data, would be 74% greater than that of the $f=19.5$ GHz data. The slight spreading in the curves may reflect an error in the exponent 1.2 or it may result from an additional component of ΔR_S from the pinned vortices denoted by $\Delta R_{S,a}$ which has a frequency dependence $\Delta R_{S,a} \propto f^2$ and is not strongly temperature dependent. The scaling in the ΔR_S data suggests that $\Delta R_S = R_{S,\mathrm{th}} + R_{S,a}$ where $\Delta R_{S,\mathrm{th}} \propto f^{1.2}$ results from the activation of vortices between metastable states and $\Delta R_{S,a}$ results from strongly pinned vortices.

V. COMPARISON WITH OTHER RELATED WORK

This work comprehensively characterizes and explains the low-temperature behavior of Z_S in high-T_c films in the mixed state at frequencies between 1 and 20 GHz as a function of temperature. We have shown that the theories for Z_S which assume uniform vortex pinning can be made to fit our data; however, while it is expected that U_P should decrease with increasing temperature[12,13,30,37,38] the fits of our data to a model which assumes a uniform pinning energy yield a U_P that must rise linearly with temperature. Further, as discussed previously, the values of $U_P \approx 7kT$ generated by the fits suggest that the low-frequency ΔR_S, and therefore the overall frequency dependence of ΔR_S, should be a strong function of temperature and sample characteristics. This is not exhibited in our data, which instead indicate that a component of $\Delta R_S \propto f^{1.2}$ is fundamental to these disordered materials in the mixed state over a broad range in temperature and frequency.

The values of α_P we determined at $f \simeq 7.3$ GHz are summarized in Table I. Both the low-temperature magnitudes and temperature dependences of α_P are similar to those obtained by other authors. Wu and Sridhar[30] found $\alpha_P(0)$ to be 2.2×10^5, Pambianchi *et al.*[4] found $\alpha_P(0)$ to be 2.7×10^5, and M. Golosovsky *et al.*[28] found $\alpha_P(0)$ to be 3.0×10^5, all in units of $\mathrm{N/m}^2$. The Wu and Sridhar[30] data imply that α_P is field independent at $B<0.1$ T. They also found that the temperature dependence of α_P at low temperatures was quadratic in agreement with Eq. (10). The present work, Golosovsky *et al.*[28] and Pambianchi *et al.*[4] all find α_P to be field independent and to have a strong linear component in the temperature dependence of α_P at low temperatures.

There has been very little previous work characterizing the frequency dependence of vortex-induced Z_S over a frequency span as large as that in the present work. Golosovsky *et al.*[28] and Pambianchi *et al.*[4] made their measurements at 5.5 GHz, and 11 GHz, respectively, and could not measure frequency dependences. However, Yeh *et al.*[31] found reasonable agreement with the Coffey-Clem model at the frequencies of 12 and 18 GHz. They studied c-axis epitaxial films of YBCO and Nd-Ce-Cu-O on $LaAlO_3$ substrates in sapphire-ring resonators and found a $\Delta R_S \propto f^2$ dependence at low temperatures. The $\Delta R_S \sim f^1$ relationship has been observed in YBCO single crystals by Wu *et al.*[43] and Fischer[44] in their measurements of the frequency dependence of high-T_c materials from 10 to 600 MHz. They where unable to fit their data to models such as the Coffey-Clem model. However, since they obtained their results near T_c, they interpreted their data in terms of vortex glass theories.[45] Wu *et al.*[46] also obtained a $\Delta R_S \sim f^1$ dependence up to frequencies of ≈ 20 GHz at temperatures near T_c and they also attributed their results to collective effects. Powell *et al.*[35] have studied the temperature dependence of Z_S at 8 and 16 GHz. They obtained a frequency and temperature dependence of ΔR_S similar to those obtained in the present work, and suggest that their results may be understandable in terms of models which include flux creep. Additionally, Revenaz *et al.*[19] in earlier work in this research group found at $T=4.2$ K the same frequency dependence for ΔR_S as that found in this work, and attributed it to flux creep resulting from a single small activation energy of roughly 40 K. The work reported here extends this early work and, because of the measured temperature dependence of the present work, additional features were required for the model to fit the data.

VI. DISCUSSION

Although the fits of the Coffey-Clem model to the frequency shift data in Fig. 3 and Fig. 4 yield reasonably good agreement if $f_P \gg 20$ GHz, the fits of this model to the ΔR_S data lead to several inconsistencies as explained below. The first inconsistency is in the behavior of the parameter f_P. In the two samples the fits of the Coffey-Clem model to the high-frequency ΔR_S data at the lowest temperature (5 K) suggest that $f_P \approx 65$ GHz. As the temperature increases, the high-frequency ΔR_S increases. In models which assume uniform vortex pinning, this requires f_P to decrease to values of <20 GHz for $T \geqslant 40$ K in sample No. 1. However, the ΔX_S vs f_n data, such as that shown in Fig. 4, directly contradict this, showing that f_P remains higher than 40 GHz for the majority of vortices in both samples for $T \leqslant 40$ K. The higher values of $f_P \sim 200$ GHz from the ΔX_S vs f_n data are consistent with the value of f_P calculated from η in Eq. (8) and the

empirically determined α_P in Eq. (19).

The second inconsistency is in the sample and temperature invariance of the frequency dependence of ΔR_S. If ΔR_S is determined by a model with a uniform pinning potential [Eq. (15)], then the low-frequency ΔR_S is determined by a single activation energy. Since $U_P \approx 7kT$, ΔR_S should have a strong exponential temperature dependence at low frequency. The high-frequency dissipation predicted by Eq. (15) should have the temperature dependence of $f_P \times \alpha_P$, which will generally be much weaker. As a result, the frequency dependence of ΔR_S should be sensitive to temperature. Because U_P should be a function of the sample characteristics, the frequency dependence of ΔR_S which is very sensitive to U_P/kT should vary significantly between samples, but our data do not exhibit these variations.

The third difficulty presented by the fits of the ΔR_S data to this model is the behavior of U_P. The fits of ΔR_S to the Coffey-Clem model accommodate the sample and temperature invariance of the frequency dependence of ΔR_S by yielding a pinning energy which rises linearly with temperature ($U_P \approx 7kT$), in contradiction to other work[12,30,37,38] and in contradiction to the T dependence we infer for $U_P(T)$ from $\alpha_P(T)$ [Eqs. (9) and (19)]. Our data suggest that the rise in U_P with T is an artifact arising from the use of a sum of $\Delta R_S \propto f^0$ and $\Delta R_S \propto f^2$ components to fit data which have a dominant $\Delta R_S \propto f^{1.2}$ behavior.

The random potential model reproduces all of the features of the frequency and temperature dependence of both R_S and X_S without any of the difficulties arising from the fits to the uniform potential model. The principal problem in the fits to the random potential model is the difference between the predicted $R_S \sim f^1$ dependence and the $R_S \sim f^{1.2}$ dependence of the data. Increasing the complexity in the functional forms of the fitting parameters, particularly $g(U_b)$, would allow more careful adjustment of the temperature dependence of Z_S but does not significantly affect the frequency dependence predicted by the model.

The $R_S \sim f$ dependence of the random potential model is common in overdamped systems with negligible mass such as the vortex system. It results from a distribution of characteristic frequencies whose contribution to χ_{ac} is approximately proportional to $1/f$. This distribution is common in disordered systems containing metastable energy states.[16,39,47–50] If the characteristic frequencies are $f_{th} = f_a \exp[-U_b/kT]$ and the probability of a given energy barrier is $g(U_b)$, then the distribution of f_{th} would be $g(U_b)/f_{th}$ so that if U_b were distributed smoothly, $\Delta R_S \sim f$. The characteristic frequencies in this model can be thought of as being determined by an activated viscosity.[48] Therefore, the frequency shift data which reflect primarily the vortex restoring force constant α_P (see Figs. 3 and 4) will not be affected significantly by this dissipation mechanism. Two principal effects which are seen in our data result from the increased vortex polarizability due to the small number of vortex segments which are thermally activated between metastable states. The first effect is a reduction in the vortex contribution to the kinetic inductance L_k with increasing frequency, since fewer vortex segments will hop between metastable states quickly enough to remain in phase with H_{rf}. This reduction in L_k results in a ΔX_S which is sublinear in f, particularly at low frequencies and higher temperatures where vortex activation is more important (Fig. 4). The second effect is that vortex activation at higher temperatures causes the measured low-frequency vortex restoring force $\alpha_P(T)$ to be smaller than that which results from the linear motion of vortices in their potential wells. As a result, the $\Delta X_S/f_n \propto 1/\alpha_P$ decreases as f increases (Fig. 3). Part of the temperature dependence in the empirically determined $\alpha_P(T)$ given by Eq. (19) results from vortex activation, and reflects the shape of the distribution $g(U_b)$.

Both this model and the fits to the Coffey-Clem model assume low values of vortex pinning energies to account for the significant levels of low frequency dissipation in these samples (see Fig. 5).[19] dc magnetization measurements and other very-low-frequency measurements of vortex dynamics tend to probe vortex displacements greater than the vortex-vortex separation $a_0 = (\phi_0/B)^{1/2}$ and therefore energies, which are generally associated with plastic deformations of the vortex lattice and yield characteristic energies[2] of ~ 5000 K. However, in the frequency range between 1.2 and 20 GHz, typical vortex displacements are much smaller and therefore the corresponding energy variations are smaller.[18] Since the value of α_P that we find from frequency shift data is independent of magnetic field, and since ΔR_S is found to increase roughly linearly with field,[16] we conclude that the pinning of the vortices is predominately due to the interaction of their cores with sample defects rather than through vortex-vortex interactions. For these reasons we conclude that the vortices studied in this work are pinned in the single-vortex limit.[19] In this limit, there has been considerable theoretical and experimental work to determine the vortex excitation energies.[3,51,52] The lattice energies which result from the motion of segments of vortex cores of length l with respect to the rest of that core are tilting energies, and are characterized by a tilt modulus[19,51,53]

$$C_{44} \approx \frac{\sqrt{3} B \phi_0}{4\pi \Gamma \mu_0 \lambda_\parallel^2}, \tag{20}$$

where $\Gamma = \lambda_\perp/\lambda_\parallel \approx 5$ is an anisotropy factor. The energy of displacement U_{tilt} of a vortex segment of length l by a distance ξ is

$$U_{tilt} \approx C_{44} V_c (\xi/l)^2, \tag{21}$$

where V_c is the correlated volume of the vortex lattice.[54] In the single-vortex limit, $V_c \approx a_0^2 l$, where $a_0 = (\phi_0/B)^{1/2}$. For $\xi < l < a_0$, U_{tilt} has typical energies of about 5–100 K.

The energies associated with the motion of vortex segments with respect to other vortices U_{shear} are even smaller than U_{tilt}. The U_{shear} are determined primarily by the vortex-lattice shear modulus.[3,51] For $\xi < l < a_0$ and for displacements of roughly ξ, these energies are only a few kelvin. Because U_{shear} and U_{tilt} are small, the interaction energies of the individual vortex cores with pinning sites in the samples are the most important. Among the mechanisms responsible for core pinning, point defects such as oxygen vacancies or

atomic interstitials have been shown to be important.[3,10–12] The density of point defects in high-T_c materials is believed to be high enough so that a segment of a vortex core will contain several such defects per copper oxide layer,[3] and the defects have volumes $D_v \ll \xi^3$ and pinning ranges $r_f \sim \xi$. The pinning energy of a point defect is small and depends on the nature of its interaction with the vortex core. In the simplest models, the pinning energy of a single defect is determined by the amount of condensation energy it displaces, $U_d \approx D_v \mu_0 B_c^2$, with a low-temperature value of about 2 K and a temperature dependence principally determined by that of B_c^2 which is given in Eq. (10) for α_P.

More sophisticated models treat the effect of quasiparticle scattering by the defects.[55,56] The scattering produces deformations of the order parameter up to lengths of $\sim \xi$, and it is energetically favorable for the strong variations of the order parameter of the vortex core to coincide with those of the defect. In these models, individual defects produce low-temperature pinning energies proportional to the defect's cross section D_a times ξ, and so $U_d \approx \xi D_a \mu B_c^2 \approx 10$ K.[12,56] This numerical value depends on the material's "dirt parameter" $\xi_0 / l_{\rm sc}$ where $l_{\rm sc}$ is the quasiparticle mean free path and $\xi_0 \approx 0.74 \xi_{\parallel}(0)$.[3] This pinning energy has a temperature dependence which is approximately equal to that of α_P in Eq. (11). At low temperatures this mechanism for vortex pinning has a temperature dependence which is similar to what we measure for α_P; however, its overall temperature dependence is too strong to explain our results (Fig. 4). The accuracy of this form for α_P relies on the relative absence of background scattering from other defects, and as the dirt parameter increases above unity, the pinning energies are reduced. The spatial dependence of a defect pinning energy is roughly[55,56] $U(r) \propto \exp\{-1.5 r^2/\xi^2\}$, and the effective pinning energy is generally taken to be determined by the variations in the defect density. A density of n defects per vortex core segment yields a mean pinning energy $\approx \sqrt{n} U_{\rm defect}$.[55,56]

The actual vortex pinning potential results from a random sum of the collective energies $U_{\rm shear}$ and $U_{\rm tilt}$ and the potential which results from the random distribution of sample point defects whose pinning range is $\approx \xi$. Therefore, it is improbable that the resulting potential is uniform as is assumed by models such as the Coffey-Clem model. The short characteristic pinning lengths and low pinning energies of randomly distributed point defects make it likely that many of the vortex segments are pinned in local energy minima which are separated from other minima by distances $\approx \xi$ and by energy barriers U_b as small as only a few kelvin. The characteristic frequencies for thermally assisted transitions between metastable states could then be in the range of the frequency of the applied rf signal for an appreciable number of vortex segments at all measured frequencies and temperatures.

A more detailed solution of the problem of a system of vortices moving between metastable states in a viscous medium would probably produce additional high-frequency losses which would modify Eq. (16) and may result in the $\Delta R_S \propto f^{1.2}$ dependence we measure rather than the $\Delta R_S \sim f^1$ predicted by Eq. (16). In addition, a more careful treatment of the effect of η on the distribution of characteristic frequencies would better define the temperature and frequency range in which the Koshelev-Vinokur model is valid.

VII. CONCLUSION

We have presented measurements of the microwave surface impedance Z_S for YBCO thin films in the mixed state. Measurements were obtained in static magnetic fields well above B_{c1} as a function of frequency from 1.2 to 22 GHz at temperatures from 5 to 65 K. Our results show that we are studying the interactions between individual vortex cores and pinning sites in the YBCO films and not collective long-range interactions between vortices. We have found in these frequency, field, and temperature ranges that most of the vortices are pinned in potentials $U_P \gg kT$ and that their motion is consistent with most theories of vortex dynamics.[13,14,16,57] These vortices oscillate in potential minima with an amplitude described by a vortex restoring force constant α_P whose temperature and field dependence is largely consistent with the previously published theories discussed above [Eqs. (10) and (11)]. However, the $\Delta R_S \propto f^2$ energy dissipation by these strongly pinned vortices is not the dominant contribution to ΔR_S in these films. Instead, a dominant $\Delta R_S \propto f^{1.2}$ is measured at all frequencies, fields, and temperatures. This frequency dependence in ΔR_S is consistent with a vortex susceptibility $\chi_{\rm ac}$ which results from an approximately $1/f$ distribution of characteristic damping frequencies. Such a distribution is common in disordered systems and results from the rates of activation over a slowly varying distribution of energy barriers between metastable system states.

We have investigated the vortex dynamics in the low-power linear regime at frequencies approaching the expected pinning frequency of $\sim 10^{11}$Hz. Since $f_{\rm th} \propto \exp -U_b/kT$ and the magnitude of $\Delta R_S(f)$ are proportional to the number of vortex segments for which $f_{\rm th} \approx f$, measurements at lower frequencies will provide insights into the number of vortex states which have a larger U_b and therefore yield information about the shape of the distribution $g(U_b)$ at higher U_b. In order to study $g(U_b)$ at higher energies, lower-frequency resonators have been designed. An extension of this work to higher-microwave-power levels would allow a separate probe of the nature of the distribution of energy barriers and the origin of the $1/f$ distribution of characteristic frequencies. As a further test of the mechanism we plan to perform measurements at lower temperatures (≤ 2 K) which will allow one to better understand the thermal diffusion of vortices.

ACKNOWLEDGMENTS

The work at MIT was supported by AFOSR Grant No. F4962-93-1-0160. The work at the Rome Laboratory was sponsored by the Department of the Air Force. At the MIT Lincoln Laboratory, the work was supported by the Advanced Research Projects Agency (ARPA) under the auspices of the Consortium for Superconducting Electronics (CSE). We wish to thank R. P. Konieczka and D. Baker for help with device fabrication, G. Fitch for help with programming, and Dr. A. C. Anderson of MIT Lincoln Laboratory for supplying the high-T_c films, for developing many of the experimental techniques used in this work, and for many helpful discussions.

[1] G. D'Anna, W. Benoit, W. Sadowski, and E. Walker, Europhys. Lett. **20**, 167 (1992).
[2] Ph. Seng, R. Gross, U. Baier, M. Rupp, D. Koelle, R. P. Huebener, P. Schmitt, G. Saemann-Ischenko, and L. Schultz, Physica C **192**, 403 (1992).
[3] C. J. van der Beek and P. H. Kes, Phys. Rev. B **43**, 13 032 (1991).
[4] M. S. Pambianchi, D. H. Wu, L. Ganapathi, and S. M. Anlage, IEEE Trans. Appl. Supercond. **AS-3**, 2774 (1993).
[5] J. Owliaei, S. Sridhar, and J. Talvacchio, Phys. Rev. Lett. **69**, 3366 (1992).
[6] T. Schuster, H. Kuhn, E. H. Brandt, M. Indenbom, M. R. Koblischka, and M. Konczykowski, Phys. Rev. B **50**, 16 684 (1994).
[7] D. E. Oates, A. C. Anderson, D. M. Sheen, and S. M. Ali, IEEE Trans. Microwave Theory Tech. **MTT-39**, 1522 (1991).
[8] D. M. Sheen, S. M. Ali, D. E. Oates, R. S. Withers, and J. A. Kong, IEEE Trans. Appl. Supercond. **AS-1**, 108 (1991).
[9] P. P. Nguyen, D. E. Oates, M. S. Dresselhaus, and G. Dresselhaus, Phys. Rev. B **48**, 6400 (1993).
[10] E. H. Brandt, Physica C **195**, 1 (1992).
[11] M. Daeumling, J. M. Seuntjens, and D. C. Larbalestier, Nature (London) **346**, 1332 (1990).
[12] E. V. Thuneberg, Cryogenics **29**, 236 (1989).
[13] M. W. Coffey and J. R. Clem, Phys. Rev. Lett. **67**, 386 (1991).
[14] E. H. Brandt, Phys. Rev. Lett. **67**, 2219 (1991).
[15] C. J. van der Beek, V. B. Geshkenbein, and V. M. Vinokur, Phys. Rev. B **48**, 3393 (1993).
[16] A. E. Koshelev and V. M. Vinokur, Physica C **173**, 465 (1991).
[17] J. I. Gittleman and R. Rosenblum, Phys. Rev. Lett. **16**, 734 (1966).
[18] M. W. Coffey and J. R. Clem, Phys. Rev. B **46**, 11 757 (1992).
[19] S. Revenaz, D. E. Oates, D. Labbe-Lavigne, G. Dresselhaus, and M. S. Dresselhaus, Phys. Rev. B **50**, 1178 (1994).
[20] A. S. Westerheim, L. S. Yu-Jahnes, and A. C. Anderson, IEEE Trans. Magn. **MAG-27**, 1001 (1991).
[21] A. S. Westerheim, A. C. Anderson, D. E. Oates, S. N. Basu, D. Bhatt, and M. J. Cima, J. Appl. Phys. **75**, 393 (1994).
[22] A. C. Anderson (private communication).
[23] D. E. Oates, A. C. Anderson, and P. M. Mankiewich, J. Supercond. **3**, 251 (1990).
[24] D. E. Oates, A. C. Anderson, C. C. Chin, J. S. Derov, G. Dresselhaus, and M. S. Dresselhaus, Phys. Rev. B **43**, 7655 (1991).
[25] Z.-D. Hao, J. R. Clem, M. W. McElfresh, L. Civale, A. P. Malozemoff, and F. Holtzberg, Phys. Rev. B **43**, 2844 (1990).
[26] N. C. Yeh, Phys. Rev. B **40**, 4566 (1989).
[27] N. C. Yeh and C. C. Tsuei, Phys. Rev. B **39**, 9708 (1989).
[28] M. Golosovsky, M. Tsindlekht, H. Chayet, and D. Davidov, Phys. Rev. B **50**, 470 (1994).
[29] M. J. Stephen and J. Bardeen, Phys. Rev. Lett. **14**, 112 (1965).
[30] D. H. Wu and S. Sridhar, Phys. Rev. Lett. **65**, 2074 (1990).
[31] N. C. Yeh, U. Kriplani, W. Jiang, D. S. Reed, D. M. Stayer, A. Gupta, A. Kussmaul, J. B. Barner, B. D. Hunt, M. C. Foote, and R. P. Vasquez, Phys. Rev. B **48**, 9861 (1993).
[32] V. M. Vinokur, G. Blatter, M. V. Feigel'man, V. B. Geshkenbein, and A. I. Larkin, Physica C **185-189**, 276 (1991).
[33] T. Penney, S. von Molnar, D. Kaiser, F. Holtzberg, and A. W. Kleinsasser, Phys. Rev. B **38**, 2918 (1988).
[34] B. A. Willemsen, S. Sridhar, J. S. Derov, and J. H. Silva, Appl. Phys. Lett. **67**, 551 (1995).
[35] J. R. Powell, A. Porch, C. E. Gough, and R. G. Humphreys, Appl. Supercond. Conf., Abstract MQC-10, p. 189, Boston, MA (Oct. 1994).
[36] P. H. Kes and C. J. van der Beek, Physica B **169**, 80 (1991).
[37] P. H. Kes, J. Aarts, J. van der Berg, C. J. van der Beek, and J. A. Mydosh, Supercond. Sci. Technol. **1**, 242 (1989).
[38] N. C. Yeh, Phys. Rev. B **43**, 523 (1991).
[39] L. B. Ioffe and V. M. Vinokur, J. Phys. C **20**, 6149 (1987).
[40] G. Müller, N. Klein, A. Brust, H. Chaloupka, M. Hein, S. Orbach, H. Piel, and D. Reschke, J. Superconduct. **3**, 235 (1990).
[41] P. P. Nguyen, D. E. Oates, G. Dresselhaus, M. S. Dresselhaus, and A. C. Anderson, Phys. Rev. B **51**, 6686 (1995).
[42] The curves were fit to the Koselev-Vinokur model without the use of a formal optimization algorithm. A fully optimized solution to the model has not yet been carried out.
[43] H. Wu, N. P. Ong, and Y. Q. Li, Phys. Rev. Lett. **71**, 2642 (1993).
[44] D. S. Fischer, Phys. Rev. B **43**, 130 (1991).
[45] M. P. A. Fischer, Phys. Rev. Lett. **62**, 1415 (1989).
[46] D. H. Wu, J. C. Booth, and S. M. Anlage, Phys. Rev. Lett. **75**, 525 (1995).
[47] W. F. Brown, Jr., in *Fluctuation Phenomena in Solids*, edited by R. E. Burgess (Academic, New York, 1965), Chap. 2, p. 37.
[48] A. K. Jonscher, *Dielectric Relaxation in Solids* (Chelsea Dielectrics Press Limited, London, 1983).
[49] L. B. Kiss, Z. Gingl, Z. Marton, J. Ketesz, F. Moss, G. Schmera, and A. Bulsara, J. Stat. Phys. **70**, 451 (1993).
[50] J. J. Brophy, in *Fluctuation Phenomena in Solids*, edited by R. E. Burgess (Academic, New York, 1965), Chap. 1, p. 1.
[51] V. M. Vinokur, P. H. Kes, and A. E. Koshelev, Physica C **168**, 29 (1990).
[52] M. V. Feigel'man, V. B. Geshenkbein, A. I. Larkin, and V. M. Vinokur, Phys. Rev. Lett. **63**, 2303 (1989).
[53] A. Sudbø and E. H. Brandt, Phys. Rev. Lett. **66**, 1781 (1991).
[54] A. I. Larkin and Y. N. Ovchinnikov, J. Low Temp. Phys. **34**, 409 (1979).
[55] E. V. Thuneberg, J. Kurkijarvi, and D. Rainer, Phys. Rev. B **29**, 3913 (1984).
[56] P. H. Kes, IEEE Trans. Magn. **MAG-23**, 1160 (1987).
[57] M. W. Coffey and J. R. Clem, Phys. Rev. B **45**, 10 527 (1992).